

LETTER

## Megawatt peak power, octave-spanning Ti:sapphire oscillators

To cite this article: Jianwang Jiang *et al* 2019 *Appl. Phys. Express* **12** 102009

View the [article online](#) for updates and enhancements.



## Megawatt peak power, octave-spanning Ti:sapphire oscillators

Jianwang Jiang<sup>1,2</sup>, Shaobo Fang<sup>2,3\*</sup>, Guoqing Chang<sup>2</sup>, Hainian Han<sup>2</sup>, Hao Teng<sup>2</sup>, and Zhiyi Wei<sup>2,3,4</sup>

<sup>1</sup>School of Physics and Optoelectronic Engineering, Xidian University, Xi'an 710071, People's Republic of China

<sup>2</sup>Beijing National Laboratory for Condensed Matter Physics, Institute of Physics, Chinese Academy of Sciences, Beijing 100190, People's Republic of China

<sup>3</sup>University of Chinese Academy of Science, Beijing 100049, People's Republic of China

<sup>4</sup>Songshan Lake Material Laboratory, Dongguan 523808, People's Republic of China

\*E-mail: [shaobo.fang@iphy.ac.cn](mailto:shaobo.fang@iphy.ac.cn)

Received June 12, 2019; revised August 23, 2019; accepted August 29, 2019; published online September 11, 2019

We demonstrate a high-power, octave-spanning, Kerr-lens mode-locked Ti:sapphire laser using double-chirped mirrors to precisely compensate for intracavity dispersion. The ultra-broadband spectrum spans from 550 nm to 1100 nm and the few-cycle pulse is as short as 6.6 fs with an average power up to 880 mW corresponding to the peak power of 1.6 MW. This is, to the best of our knowledge, the highest average output power directly achieved from an octave-spanning Ti:sapphire laser oscillator at the repetition rate of 80 MHz. In addition, the third-order harmonically mode-locked phenomenon was observed in our experiments. © 2019 The Japan Society of Applied Physics

**T**itanium-doped sapphire (Ti:sapphire,  $\text{Ti:Al}_2\text{O}_3$ ) has been an excellent gain crystal for producing near-infrared femtosecond laser pulses because of its superior optical, thermodynamic and mechanical properties.<sup>1,2)</sup> In the past few decades, Ti:sapphire lasers are able to emit sub-10-fs pulses with an octave-spanning spectrum thanks to the invention of Kerr-lens mode-locking (KLM) technology and double-chirped mirrors (DCMs).<sup>3-5)</sup> Octave-spanning Ti:sapphire lasers are widely used for frequency comb,<sup>6)</sup> generation of isolated attosecond pulses,<sup>7-9)</sup> broadband spectroscopy,<sup>10)</sup> excitation of multiple fluorescence proteins<sup>11)</sup> and so on.<sup>12)</sup>

To date, three methods have been reported to generate an ultra-broadband spectrum from a Ti:sapphire oscillator. The first approach is usually to employ the strong nonlinear effects in a photonic crystal fiber (PCF) to generate an octave-spanning spectrum outside the resonant cavity.<sup>13-16)</sup> However, due to the low damage threshold of the PCF end facets and the relatively low coupling efficiency, it is difficult to deliver an octave-spanning spectrum with high average power. The coherence of the supercontinuum is usually reduced because of additional amplitude-to-phase noise induced by the complex nonlinear processes in fiber. Moreover, the complicated coupling mechanism and the accumulated heat on the PCF end facets degrade the long term stability. The second approach is to combine DCMs with prism pairs inside the cavity for fine tuning the intracavity dispersion to achieve an ultra-broadband spectrum and shorter pulse.<sup>17-19)</sup> However, insertion of the prism pairs may cause high order dispersion, which cannot be fully compensated by DCMs. Due to the long distance between the prism pair, it is also hard to increase the laser repetition rate to more than 200 MHz. The third approach is to use DCMs for dispersion compensation in the resonator.<sup>20)</sup> DCMs have higher reflectivity, large dispersion, and are easy to align. A pair of small-angle wedges is usually inserted into the optical path for dispersion fine tuning. In 2001, an octave spanning Ti:sapphire laser with 120 mW output power was first reported by Ell et al., which utilized additional self-phase modulation in a BK7 plate inside the cavity.<sup>21)</sup> Then, Matos et al. described an octave-spanning, prismless Ti:sapphire laser with the phase stabilization, but the average power was only 90 mW under the mode-locked operation.<sup>22)</sup> Zhang et al. reported an octave-spanning Ti:sapphire oscillator with

output power of 200 mW in 2012.<sup>23)</sup> Most recently, Yu et al. reported an octave-spanning Ti:sapphire laser with the maximum power of 320 mW, which was developed as a monolithic optical comb.<sup>24)</sup> Although, there are many approaches to generate an ultra-broadband spectrum,<sup>25-27)</sup> the high output power close to watt-level has been a challenge. The typical average output power of octave-spanning Ti:sapphire lasers is usually below 400 mW, which limits the feasible applications in many fields. A high-power octave-spanning laser oscillator has been applied for a monolithic optical comb to improve the signal-to-noise ratio (SNR) of beat signal where the different frequency crystal MgO:PPLN can handle higher power.<sup>28,29)</sup> Higher average power also benefits frequency comb spectroscopy. Furthermore, high power lasers with one octave spectrum can be utilized to surface second harmonic generation in some two-dimensional materials (e.g., graphene).<sup>30,31)</sup>

In this letter, we use specially designed DCMs to precisely compensate for intracavity dispersion and implement a high-power, octave-spanning, Kerr-lens mode-locked Ti:sapphire laser oscillator. The laser delivers 6.6 fs pulses with 0.88-W average output power and an ultra-broadband spectrum covering from 550 nm to 1100 nm. This is, to the best of our knowledge, the highest output power directly delivered from a Ti:sapphire oscillator at the repetition rate of 80 MHz.

The schematic experimental setup is shown in Fig. 1. A typical astigmatically compensated Z-fold eight-mirror cavity is adopted. The total length of cavity is 1874 mm, in which the long and short arm are 1254 and 624 mm respectively, corresponding to the repetition rate of 80 MHz. Two folding mirrors M5 and M6 with a radius of curvature (ROC) of 75 mm are utilized to increase the power intensity in the crystal. We estimated the intracavity beam waist is  $8.2 \times 9.6 \text{ um}^2$  ( $1/e^2$ ) under the ABCD matrix analysis. The pump laser was focused onto the Ti:sapphire crystal by a lens with the focal length of 50 mm. The waist radii of the pump laser were measured to be  $7.6 \times 8.1 \text{ um}^2$  ( $1/e^2$ ) by a commercial CCD camera. A diode-pumped, frequency-doubled CW laser capable of providing a maximum output power of 15 W at 532 nm was chosen as the pump source. A 2-mm-long, Brewster-angle-cut Ti:sapphire crystal with  $\alpha_{532} = 7.3 \text{ cm}^{-1}$  and figure of merit (FOM)  $> 100$  was employed as the active medium whose single-pass absorption coefficient was 75% at 532 nm. To reduce the accumulated heat in the Ti:sapphire

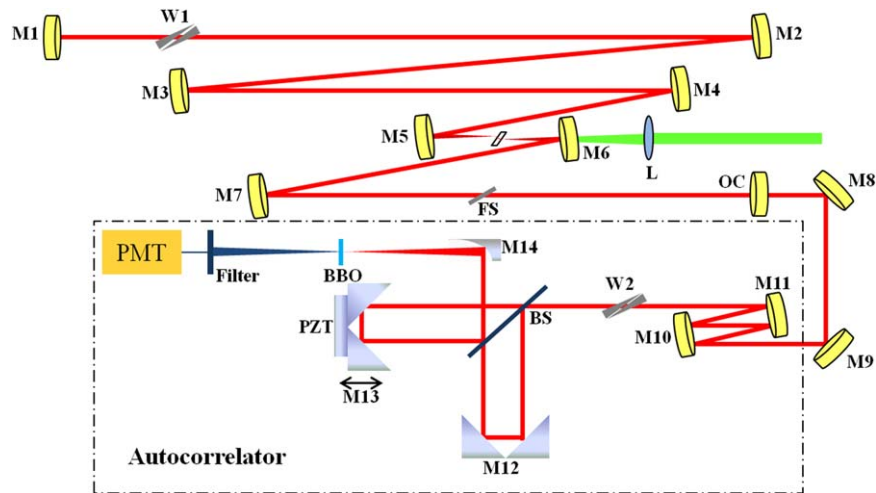


**Fig. 1.** (Color online) Experimental setup of the high-power octave-spanning Ti:sapphire laser. Three pairs of DCMs (M2–M7) with smooth average are used in the cavity. M5, M6: plane-concave chirped mirror pair with ROC of 75 mm, OC: output coupler with transmittance of 20%, L: pump lens ( $f = 50$  mm), FS: fused silica plate, W1, W2: a pair of fused silica wedges, M1, M8, M9: plane silver mirror. M10, M11: DCM, BS: beam splitter, M14: off-axis parabolic mirror coated with gold film. BBO: barium metaborate crystal with the thickness of  $20 \mu\text{m}$ . PMT: photomultiplier tube.

crystal and keep a stable operation, the Ti:sapphire crystal was wrapped with indium foil and mounted tightly on a water-cooled copper heat sink block kept at  $18^\circ\text{C}$  during the experiment. Two concave spherical mirrors of M5 and M6 were coated with high reflectivity over 99.9% in the range of 600–1080 nm and high transmission at 532 nm as pump mirrors. Moreover, in order to generate sub-10-fs pulse directly, three pairs of double-chirped mirror pairs (M2–M7) were employed in the cavity to provide ultra-broadband negative second-order dispersion. The group dispersion delay (GDD) of the M2 and M3 oscillates around  $-45 \text{ fs}^2$ , but the average GDD is very smooth between 650 nm to 1100 nm. The average GDD of the M4 and M5 is around  $-55 \text{ fs}^2$  at 650–1150 nm, and M6 and M7 have  $-55 \text{ fs}^2$  of the flat average GDD ranging from 600 nm to 1200 nm. For the purpose of increasing the average output power, a 0.5-mm-thin specially designed output coupler (OC) with high transmittance of 20% at 600–1000 nm was employed in the cavity. A plane silver mirror (M1) was placed on a translation stage as the end mirror. Meanwhile, a pair of fused silica (FS) wedges (W1) and a 1-mm-thick FS plate were used to finely compensate the intracavity dispersion. The schematic diagram of the autocorrelator for measuring the pulse duration is shown in the dotted line of Fig. 1.

First, we calculate the dispersion of common material and the net dispersion in the cavity, as displayed in Fig. 2. The net dispersion in the cavity is approximately  $-20 \text{ fs}^2$  ranging from 640 nm to 1100 nm, which is the key for achieving stable octave-spanning mode-locking. The laser cavity was aligned carefully to ensure operation at the fundamental  $\text{TEM}_{00}$  mode. The maximum CW output power is 1.2 W with a 20% output coupler under 5.5-W pump power. The KLM laser operation was realized by carefully adjusting the position of chirped mirror M5 and the crystal to the edge of the stable region. Fast shaking end mirror M1 initiated stable mode-locked operation that delivers a stable pulse train with a repetition rate of 80 MHz detected by a fast photodiode and a digital oscilloscope.

In order to further characterize the mode locking performance, we measured the output power at different pump

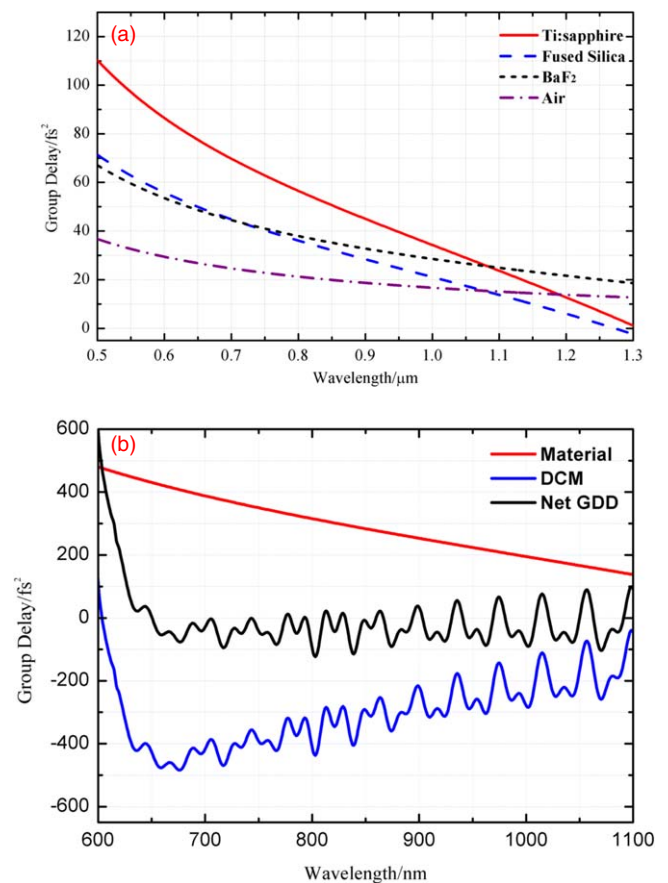


**Fig. 2.** (Color online) Calculated unit dispersion of common material curve (a) and net dispersion curve of the intra-cavity component.

power, as shown in Fig. 3. The beam profile under the maximum output power is shown in the insert of Fig. 3. The highest mode-locked average power of 0.88 W is achieved at the pump power of 5.5 W. The slope efficiency is calculated to be 20.1%. Further increasing pump power leads to multi-pulsing.

By optimizing the position of the pump mirror M5 and the Ti:sapphire crystal, as well as the insertion of FS wedge pairs W1, we obtained ultra-broadband and smooth spectrum

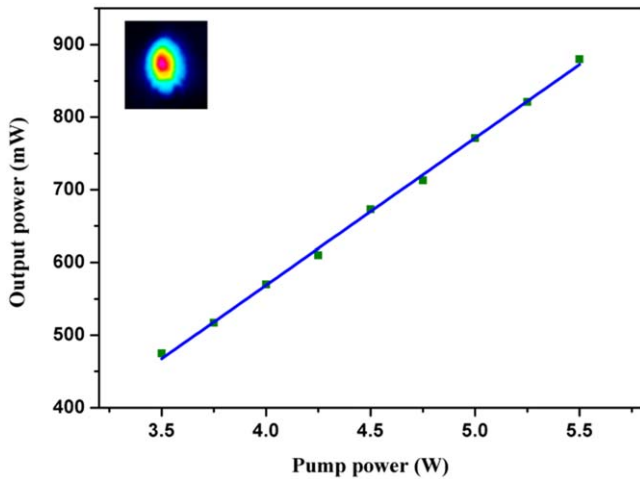


**Fig. 3.** (Color online) Mode-locked average power at different pump power. Inset: beam profile measured by a commercial CCD camera.

spanning from 550 nm to 1100 nm centered at 760 nm (Fig. 4). The interferometric autocorrelation trace is measured by a second-order autocorrelator. Chirped mirror M10 and M11 with smooth average GDD of  $-60 \text{ fs}^2$  from 550 nm to 1080 nm was used to pre-compensate for the dispersion of OC, air and BS outside the cavity. The inserted length of W2 is changed for optimization of pulse duration. The results in Fig. 5 showed that the pulse duration is 6.6 fs, which slightly deviates from Fourier-transform-limited pulse duration of 5.3 fs. Both smooth wings in the autocorrelation trace indicated the nice compensation of third-order dispersion. We believed that even shorter pulse duration could be obtained by fine dispersion compensation outside the cavity.

Using a radio-frequency (RF) spectrum analyzer and a photodetector (PD), we measured the RF power spectrum, as shown in Fig. 6. An SNR of 89 dB of the fundamental 80 MHz repetition rate was recorded in a frequency span of 20 MHz with a resolution bandwidth (RBW) of 1 kHz, as shown in Fig. 6(a). Figure 6(b) described several harmonics of repetition frequency in a frequency span from 0 to 1 GHz under the RBW of 100 kHz. The RF power spectrum in Fig. 6(b) illustrated that the stable KLM operation was realized without multi-pulse operation. The decrease of the

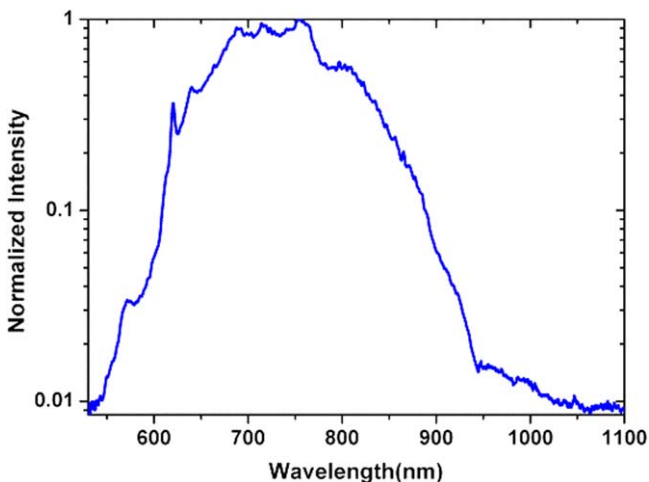


**Fig. 4.** (Color online) Typical output spectrum of the high-power Ti:sapphire laser, covering from 550 nm to 1100 nm.

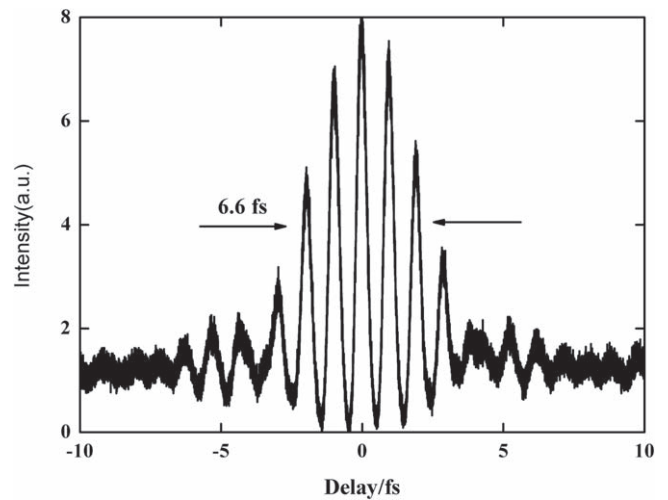


**Fig. 5.** Measured autocorrelation trace from the Ti:sapphire laser, corresponding to the pulse duration of 6.6 fs.

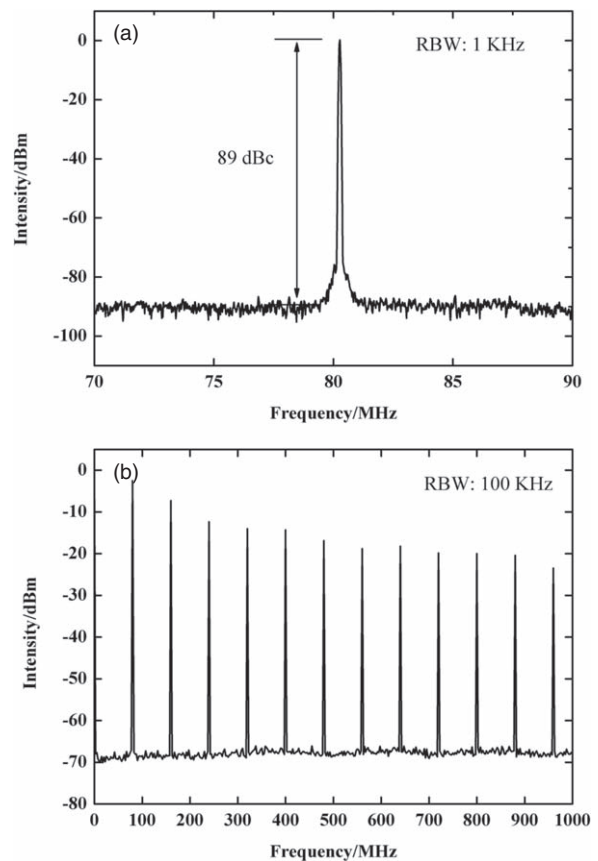


**Fig. 6.** The RF power spectrum of pulse train detected with a 1 GHz photo detector: with a resolution bandwidth of 1 kHz at the fundamental repetition rate of 80 MHz (a) and full spectrum up to 1 GHz with 100 kHz resolution (b).

harmonics peaks in Fig. 6(b) might be originated from the limited frequency response of the RF spectrum analyzer.

In addition, the harmonically mode-locked phenomenon is observed in our experiments, which is common in fiber lasers. The third-order harmonically mode-locked pulse at a repetition of 240 MHz was obtained, as showed in Fig. 7, when the M5 and Ti:sapphire crystal was adjusted to the proper position. The harmonically mode-locked pulses were established when multiple soliton with same amplitude propagate periodically in the cavity. Meanwhile, the phase

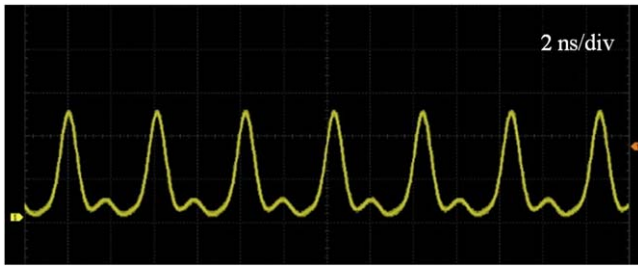


**Fig. 7.** (Color online) Oscilloscope traces of the harmonically mode-locked pulse trains in the time scales of  $2 \text{ ns div}^{-1}$ .

difference of the adjacent soliton pulse is equal to  $2\pi$ . It is beneficial for generating femtosecond pulses at ultra-high repetition rate.

**Acknowledgments** This work is supported by the National Key R&D Program of China (2017YFC0110301); National Natural Science Foundation of China (61575219, 61210017, 11774234, 11674386, 11434016, 91850209); Strategic Priority Research Program of the CAS (XDB23030230, XDB21010400, XDA1502040404); Youth Innovation Promotion Association of the CAS (2018007).

- 1) P. F. Moulton, *JOSA. B* **3**, 125 (1986).
- 2) A. Sanchez, A. J. Strauss, R. L. Aggarwal, and R. E. Fahey, *IEEE Journal of Quantum Electronics* **24**, 995 (1988).
- 3) D. E. Spence, P. N. Kean, and W. Sibbett, *Opt. Lett.* **16**, 42 (1991).
- 4) T. Brabec, C. Spielmann, and F. Krausz, *Opt. Lett.* **16**, 1961 (1991).
- 5) T. Brabec and F. Krausz, *Reviews of Modern Physics* **72**, 545 (2000).
- 6) S. A. Diddams, D. J. Jones, J. Ye, S. T. Cundiff, J. L. Hall, J. K. Ranka, R. S. Windeler, R. Holzwarth, T. Udem, and T. W. Hansch, *Phys. Rev. Lett.* **84**, 5102 (2000).
- 7) M. Hentschel, R. Kienberger, C. Spielmann, G. A. Regde, N. Milosevic, P. Corkum, U. Heinzmann, M. Drescher, and F. Krausz, *Nature* **414**, 509 (2001).
- 8) A. Baltuška et al., *Nature* **421**, 611 (2003).
- 9) E. Goulielmaris, V. S. Yakovlev, A. L. Cavalieri, M. Uiberacker, V. Pervak, A. Apolonski, R. Kienberger, U. Kleineberg, and F. Krausz, *Science* **317**, 769 (2007).
- 10) J. Du, K. Nakata, Y. Jiang, E. Tokunaga, and T. Kobayashi, *Opt. Express* **19**, 22480 (2011).
- 11) J. Livet, T. A. Weissman, H. Kang, R. W. Draft, J. Lu, R. A. Bennis, J. R. Sanes, and J. W. Lichtman, *Nature* **450**, 56 (2007).
- 12) A. D. Ludlow, M. M. Boyd, J. Ye, E. Peik, and P. O. Schmidt, *Reviews of Modern Physics* **87**, 637 (2015).
- 13) J. C. Knight, T. A. Birks, P. S. J. Russell, and D. M. Atkin, *Opt. Lett.* **22**, 7 (1997).
- 14) A. M. Heidt, A. Hartung, G. W. Bosman, P. Krok, E. G. Rohwer, H. Schwoerer, and H. Bartelt, *Opt. Express* **19**, 3775 (2011).
- 15) J. Bethge, A. Husakou, F. Mitschke, F. Noack, U. Griebner, G. Steinmeyer, and J. Herrmann, *Opt. Express* **18**, 6230 (2010).
- 16) S. Demmler, J. Rothhardt, A. M. Heidt, A. Hartung, E. G. Rohwer, H. Bartelt, J. Limpert, and A. Tunnermann, *Opt. Express* **9**, 20151 (2011).
- 17) I. D. Jung, F. X. Kärtner, N. Matuschek, D. H. Sutter, F. Morier-Genoud, G. Zhang, U. Keller, V. Scheuer, M. Tilsch, and T. Tschudi, *Opt. Lett.* **22**, 1009 (1997).
- 18) U. Morgner, F. X. Kärtner, S. H. Cho, Y. Chen, H. A. Haus, J. G. Fujimoto, E. P. Ippen, V. Scheuer, G. Angelow, and T. Tschudi, *Opt. Lett.* **24**, 411 (1999).
- 19) T. M. Fortier, D. J. Jones, and S. T. Cundiff, *Opt. Lett.* **28**, 2198 (2003).
- 20) A. Stingl, M. Lenzner, C. Spielmann, F. Krausz, and R. Szepöcs, *Opt. Lett.* **20**, 602 (1995).
- 21) R. Ell, U. Morgner, F. X. Kartner, J. G. Fujimoto, E. P. Ippen, M. J. Lederer, A. Boiko, and B. Luther-Davies, *Opt. Lett.* **26**, 373 (2001).
- 22) L. Matos, D. Kleppner, O. Kuzucu, T. R. Schibli, J. Kim, E. P. Ippen, and F. X. Kaertner, *Opt. Lett.* **29**, 1683 (2004).
- 23) L. Zhang, H. Han, Q. Zhang, and Z. Wei, *Chin. Phys. Lett.* **29**, 114208 (2012).
- 24) Z. Yu, H. Han, Y. Xie, H. Teng, Z. Wang, and Z. Wei, *Chin. Phys. B* **25**, 044205 (2016).
- 25) S. Fang, K. Yamane, J. Zhu, C. Zhou, Z. Zhang, and M. Yamashita, *IEEE Photonics Technology Letters* **23**, 688 (2011).
- 26) C. Manzoni, O. D. Mücke, G. Cirmi, S. Fang, J. Moses, S. Huang, K. Hong, G. Cerullo, and F. X. Kärtner, *Laser & Photonics Reviews* **9**, 129 (2015).
- 27) O. D. Mücke et al., *IEEE J. Sel. Top. Quantum Electron.* **21**, 8700712 (2015).
- 28) T. Fuji et al., *Opt. Lett.* **30**, 332 (2005).
- 29) T. Fuji, A. Apolonski, and F. Krausz, *Opt. Lett.* **29**, 632 (2004).
- 30) S. Chu, T. Liu, C. Sun, C. Lin, and H. Tsai, *Opt. Express* **11**, 933 (2003).
- 31) W. Zhang, L. Li, Z. B. Wang, A. A. Pena, D. J. Whitehead, M. L. Zhong, Z. Lin, and H. W. Zhu, *Appl. Phys. A* **109**, 291 (2012).